CANCER IMMUNOLOGY

Intratumoral antigen signaling traps CD8$^+$ T cells to confine exhaustion to the tumor site

Munetomo Takahashi[1,2]†, Tsz Y. So[1,3]†, Vitalina Chamberlain-Evans[1], Robert Hughes[1], Juan Carlos Yam-Puc[1], Katarzyna Kania[3], Michelle Ruhle[3], Tiffeney Mann[1], Martijn J. Schuijs[3], Paul Coupland[3,4], Dean Naisbitt[5], Timotheus Y. F. Halim[3], Paul A. Lyons[6,7], Pietro Lio[8], Rahul Roychoudhuri[9], Klaus Okkenhaug[9], David J. Adams[10], Ken G. C. Smith[6,7,11,12], Duncan I. Jodrell[13], Michael A. Chapman[1,14]‡, James E. D. Thaventhiran[1,3]‡*

Immunotherapy advances have been hindered by difficulties in tracking the behaviors of lymphocytes after antigen signaling. Here, we assessed the behavior of T cells active within tumors through the development of the antigen receptor signaling reporter (AgRSR) mouse, fate-mapping lymphocytes responding to antigens at specific times and locations. Contrary to reports describing the ready egress of T cells out of the tumor, we find that intratumoral antigen signaling traps CD8$^+$ T cells in the tumor. These clonal populations expand and become increasingly exhausted over time. By contrast, antigen-signaled regulatory T cell (T_{reg}) clonal populations readily recirculate out of the tumor. Consequently, intratumoral antigen signaling acts as a gatekeeper to compartmentalize CD8$^+$ T cell responses, even within the same clonotype, thus enabling exhausted T cells to remain confined to a specific tumor tissue site.

INTRODUCTION

CD8$^+$ T cell exhaustion is an epigenetically propagated (*1*, *2*), temporally increasing (*3*) permanent state of hypofunction that prevents damaging immune responses (*4*, *5*). Studies using elegant parabiosis experiments (*6*, *7*) and Kaede mice (*8*, *9*) have shown exhausted CD8$^+$ T cells resident in tumor tissue. These findings corroborate reports of exhausted T cells expressing CD103 (a key protein in T cell residency) (*10*, *11*) and reports of tumor-reactive cells being largely confined to the tumor (*12*, *13*). Recent studies have also observed the egress of CD8$^+$ T cells, including antigen-specific T cells, out of the tumor (*8*, *9*). Consequently, it remains unclear what precise factors regulate CD8$^+$ T cell tumor residency and egress.

Upon receipt of antigen signals, naïve T cells undergo clonal expansion to form clonotypes. The subsequent antigen signals they encounter remain pivotal in modulating their responses. Because antigen signaling is contingent on the timing and location of interaction, its effect varies for individual cells. Accordingly, antigen signaling could play a role in segregating the functional response of T cells, including regulating the residency or egress behaviors of cells from the same clonotype (*7*, *9*). Current tools to track lymphocyte responses in vivo, primarily using T cell receptor (TCR) transgenic lymphocytes (*14*–*16*) and tetramers (*17*, *18*), cannot distinguish whether, where, and when a T cell has received antigen signals. As a result, an alternative approach that tracks the effect of antigen signaling would help in validating its role in regulating CD8$^+$ T cell tumor residency and egress.

RESULTS

Developing the antigen receptor signaling reporter mouse to fate-map antigen-signaled T cells

We created the antigen receptor signaling reporter (AgRSR) mouse to enable a repertoire-wide assessment of clones that are contemporaneously TCR-signaled, including from tissues in which their cells are rare. In the AgRSR mouse the *Nur77* promoter, which is only active in T lymphocytes upon TCR ligation (*19*, *20*), drives equimolar expression of a red fluorescent protein (Katushka) and Cre-ERT2 recombinase (Fig. 1A). Crossing AgRSR mice to Rosa-Lox-Stop-Lox (LSL)–enhanced yellow fluorescent protein (EYFP) strains generates AgRSR-LSL-EYFP mice in which the transgenic system acts as a molecular AND gate that permanently marks the T cells and their progeny that have received coincident TCR and tamoxifen signals with EYFP (Fig. 1B). We first crossed the AgRSR strain to the ovalbumin (OVA)–specific OT-I TCR transgenic strain, for which variant peptide ligands of the TCR have been characterized (*21*). Naïve CD8$^+$ T cells from these animals were stimulated with OVA peptide variants in vitro. Consistent with results from a previous *Nur77-GFP* (*19*) strain, the level of Katushka induced by each ligand directly correlated with its stimulatory activity (Fig. 1, C and D), indicating that Katushka expression is dependent on the strength of TCR signaling. Next, to validate the TCR-pMHC (peptide major histocompatibility complex) dependence of EYFP expression in vivo, we transferred splenocytes from AgRSR animals into B2m knockout (KO) and RAG2 KO host mice (Fig. 1E and fig. S10A). In these CD8$^+$ T cell–deficient strains,

[1]Medical Research Council Toxicology Unit, University of Cambridge, Gleeson Building, Tennis Court Road, Cambridge CB2 1QR, UK. [2]Graduate School of Medicine and Faculty of Medicine, University of Tokyo, Tokyo 113-0033, Japan. [3]University of Cambridge, CRUK Cambridge Institute, Cambridge CB2 0RE, UK. [4]Altos Labs Cambridge Institute, Cambridge CB21 6GP, UK. [5]Department of Pharmacology and Therapeutics, University of Liverpool, Sherrington Building, Ashton Street, Liverpool L69 3G, UK. [6]Cambridge Institute of Therapeutic Immunology and Infectious Disease, University of Cambridge, Jeffrey Cheah Biomedical Centre, Cambridge Biomedical Campus, Cambridge, UK. [7]Department of Medicine, University of Cambridge, School of Clinical Medicine, Cambridge Biomedical Campus, Cambridge, UK. [8]Department of Computer Science and Technology, University of Cambridge, Cambridge CB3 0FD, UK. [9]Department of Pathology, University of Cambridge, Cambridge, UK. [10]Experimental Cancer Genetics, Wellcome Sanger Institute, Hinxton, Cambridgeshire CB10 1SA, UK. [11]Walter and Eliza Hall Institute of Medical Research, Parkville, VIC 3052, Australia. [12]University of Melbourne, Parkville, VIC 3052, Australia. [13]Department of Oncology, University of Cambridge, School of Clinical Medicine, Cambridge Biomedical Campus, Box 197, Cambridge CB2 0XZ, UK. [14]Department of Hematology, University of Cambridge, Cambridge CB2 0RE, UK.
*Corresponding author. Email: jedt2@cam.ac.uk
†These authors contributed equally to this work.
‡These authors contributed equally to this work.

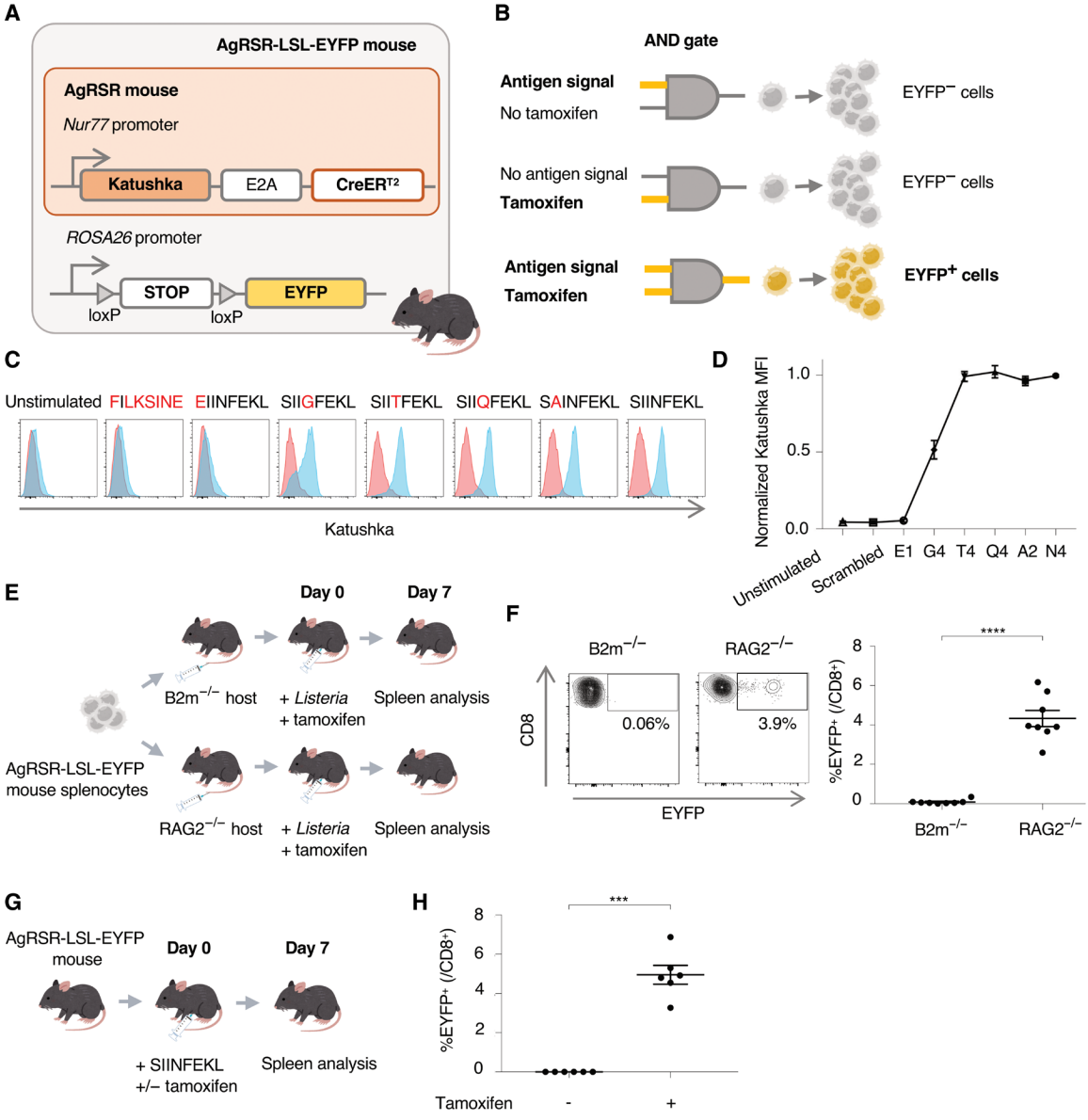

Fig. 1. The AgRSR mouse fate-maps antigen-signaled CD8$^+$ T cells. (**A**) Transgenes in the AgRSR and AgRSR-LSL-EYFP mouse. (**B**) Lymphocytes received antigen and tamoxifen signaling, and their progenies were marked EYFP$^+$. (**C** and **D**) Range of Katushka expression of OT-I × AgRSR-LSL-EYFP and WT CD8$^+$ T cells after stimulation with SIINFEKL variant peptides, by flow cytometry histograms (C) and normalized fluorescence (D). Data are representative of two independent experiments. (**E**) AgRSR-LSL-EYFP splenocytes were adoptively transferred to B2m$^{-/-}$ and RAG2$^{-/-}$ strains, challenged with *Listeria*, and tamoxifen-treated. (**F**) Representative flow cytometry plots of splenocytes at day 7 after infection (left) and summary plot of all mice (right). Data are pooled from two independent experiments ($n = 7$ per condition). (**G**) AgRSR-LSL-EYFP mice were immunized with SIINFEKL with or without tamoxifen. (**H**) Summary plot of all mice. Data are pooled from three independent experiments ($n = 6$ per condition). Dots represent mice (F and H). Data are shown as means ± SEM (D, F, and H). Statistical testing via unpaired two-tailed Student's *t* test (****$P < 0.0001$; ***$P < 0.001$).

the MHC-I TCR ligand is absent in the B2m but present in the RAG2 KO animals. Recipient mice infected with *Listeria* and treated with tamoxifen showed EYFP$^+$ fluorescence in CD8$^+$ T cells from the RAG2 KO but not the B2m KO recipients (Fig. 1F). This confirmed that EYFP expression was dependent on physiological TCR signaling caused by pMHC-I ligation rather than other inflammatory signals present in *Listeria*-infected mice. Equivalent assays to test the specificity of labeling to MHC-II antigen receptor signals were performed for CD4$^+$ T cells (fig. S1, A and B). Last, we validated EYFP expression dependence on tamoxifen signals. EYFP expression was only detected in CD8$^+$ T cells of tamoxifen-treated mice, with no detectable fluorescence in the absence of tamoxifen (Fig. 1, G and H). By temporally staggering injection of TCR-activated CD8$^+$ T cells into tamoxifen-treated mice, we assessed the duration of tamoxifen signal–inducing EYFP expression in vivo. In line with previous studies (*22*), the majority of CD8$^+$ T cells were EYFP labeled within a 48-hour window after tamoxifen injection, with no EYFP labeling occurring 72 hours after tamoxifen injection (fig. S2, A and B). Together, these results demonstrate the ability of the AgRSR mouse to fate-map T cells on coincident TCR and tamoxifen signals in vivo.

The YUMMER1.7 melanoma model provides a neoantigen-rich persistent immunological challenge that has been used for the characterization of $CD8^+$ T cell responses during immunotherapy (*23*–*25*). We used the model to investigate the effect of antigen signaling on T cell responses. When implanted, tumors grew consistently in tamoxifen-treated AgRSR mice (fig. S3A). Only AgRSR mice receiving tamoxifen after, and not before, tumors became palpable showed elevated $CD8^+$ T cell tumor $EYFP^+$ frequency (Fig. 2, A and B, and fig. S10B). In tumor-bearing mice, splenic $EYFP^+$ $CD8^+$ T cells expressed programmed cell death protein 1 (PD-1) and tumor $EYFP^+$ $CD8^+$ T cells were PD-1^{Hi} (Fig. 2, C and D), indicating substantial EYFP enrichment of T cells responding to tumor antigens in both populations (*26*, *27*). We quantified the longitudinal changes in the $EYFP^+$ frequency of $CD8^+$ T cells in the secondary lymphoid system and tumor (Fig. 2E). $EYFP^+$ frequencies expanded in all compartments, with particularly high $EYFP^+$ frequency expansion observed in the tumor (Fig. 2F). This heightened expansion could be due to direct labeling of intratumorally antigen-signaled cells, in which a subset of cells within a clonotype that receives TCR signals in the tumor is labeled $EYFP^+$. To assess whether tamoxifen was labeling subsets of clonotypes or whole clonotypes, we performed bulk TCR sequencing (TCR-seq) of $CD8^+$ $EYFP^+$ and $CD8^+$ $EYFP^-$ cells 8 days after tamoxifen administration (fig. S3B). Because naïve T cells carry a unique TCR sequence inherited by progenies during clonal expansion, checking for TCR overlap between the $EYFP^+$ and $EYFP^-$ compartments would indicate the extent of clonotype labeling. Most cells from the $EYFP^+$ compartment shared TCR sequences with cells from the $EYFP^-$ compartment across all tissues (fig. S3C), indicating EYFP

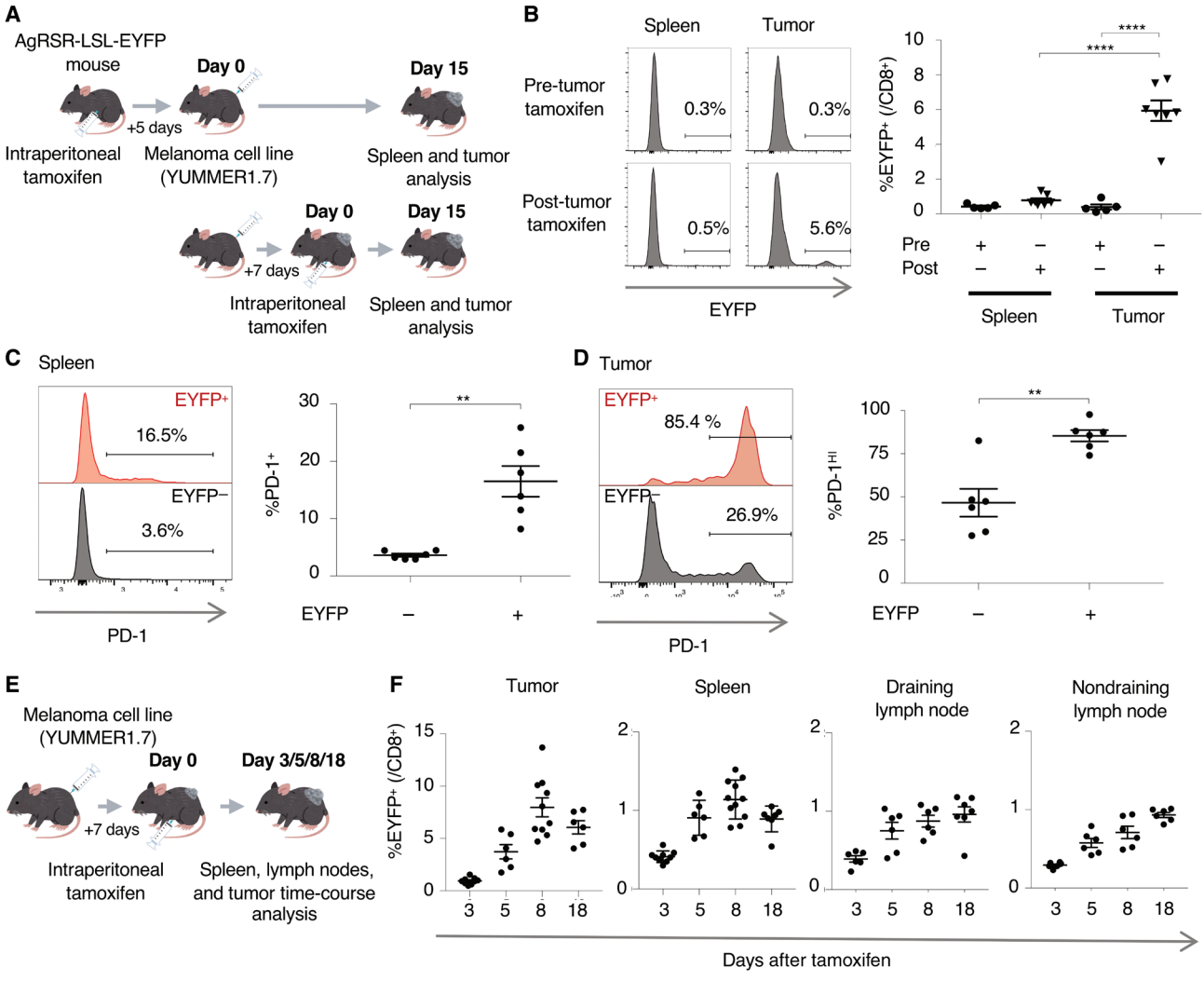

Fig. 2. The AgRSR mouse tracks the expansion of antigen-signaled $CD8^+$ T cells in the tumor immune response. (**A**) AgRSR-LSL-EYFP mice were tamoxifen-treated pre- (5 days before) or post-subcutaneous (7 days after) injection of YUMMER1.7 melanoma cells, and $CD8^+$ T cells were assessed 15 days later. (**B**) Representative flow cytometry histograms (left) and summary plots of all experiments (right). Data were pooled from two independent experiments ($n \geq 5$ per condition). (**C** and **D**) Representative flow cytometry histograms (left) and summary plots (right) of PD-1 expression in $CD8^+$ T cells from spleens (C) and tumors (D) 8 days after tamoxifen labeling. Data were pooled from two independent experiments ($n = 6$). (**E**) AgRSR-LSL-EYFP mice were implanted with YUMMER1.7 melanoma cells and treated with tamoxifen 7 days later, and $CD8^+$ T cells from spleens, tumors, draining lymph nodes, and nondraining lymph nodes were sampled at indicated days. (**F**) $EYFP^+$ percentages of $CD8^+$ T cells in the indicated tissues. Data were pooled from four independent experiments ($n \geq 5$ per condition). Dots represent mice (B to D and F). Data are shown as means ± SEM (B to D and F). Statistical testing via paired two-tailed Student's *t* test and ordinary one-way ANOVA (****$P < 0.0001$; **$P < 0.01$).

labeling capturing subsets of clonotypes. Together, these results demonstrate the AgRSR system's ability to characterize the consequences of antigen signaling in the tumor immune response.

CD8$^+$ T cell exhaustion is confined to the tumor site

To investigate the differentiation of antigen-signaled T cells at both the effector site and the circulating immune system, we analyzed sorted EYFP$^+$ T cells from tumors and spleens of four mice by paired single-cell RNA sequencing (scRNA-seq) and TCR-seq 8 days after tamoxifen injection (Fig. 3A). The TCR sequence provided a genetic barcode, which, in conjunction with EYFP labeling, enabled identification of T cell clonal expansions after antigen signaling ("antigen-signaled clonal populations"). In the dataset, most EYFP$^+$ cells from the spleen were nonexpanded, whereas most EYFP$^+$ cells from the tumor were members of expanded antigen-signaled clonal populations (fig. S4A). In the largest (>15 cells) antigen-signaled clonal populations (Fig. 3B), CD8$^+$ and CD4$^+$ T cell clonal populations could be readily distinguished by their *Cd8a* and *Cd4* expression (fig. S4, B and C). Antigen-signaled CD4$^+$ T cell clonal populations were further filtered on the basis of the proportion of cells expressing *Foxp3* (fig. S4D). We focused on a subset of CD4$^+$ regulatory T cell (T_{reg}) clonal populations that consistently expressed *Foxp3*. *Foxp3*-expressing cells from these clonal populations highly expressed genes associated with the T_{reg} state (including *Foxp3*, *Helios*, and *Nrp1*) (fig. S4E).

We first compared the differentiation states of antigen-signaled CD8$^+$ T cell clonal populations across the spleen and the tumor. Individual CD8$^+$ T cells were scored for exhaustion and cytotoxicity signatures on the basis of their up-regulation of exhaustion and cytotoxicity-associated genes (*28*) against a control group of genes (*29*). For antigen-signaled CD8$^+$ T cell clonal populations distributed across spleens and tumors, cells within the tumors had reduced cytotoxicity and elevated exhaustion scores relative to their counterparts within the lymphoid tissue (Fig. 3, C and D). Correspondingly, cells defined by their gene expression to be in a cycling phase had higher exhaustion scores in the tumor than in the lymphoid tissue (Fig. 3E). These observations were consistent in individual mice (fig. S5A) and reproduced when we used exhaustion gene sets obtained in different immune settings (fig. S5B) (*30*–*32*). In a human lung cancer dataset (*33*), tumor-infiltrating CD8$^+$ T cell clonal populations that did not have cells detectable in blood had higher exhaustion scores than counterpart populations that had cells detectable in blood (fig. S5C). In line with observations in mice, clonal populations that were detectable in blood had higher exhaustion scores in the tumors than in blood (fig. S5D). Together, these data are consistent with the containment of CD8$^+$ T cell exhaustion at the tumor site. We next compared the effector T_{reg} state of T_{regs} clonal populations across spleens and tumors by using an effector T_{reg} differentiation signature (*34*). In parallel to antigen-signaled CD8$^+$ T cell clonal

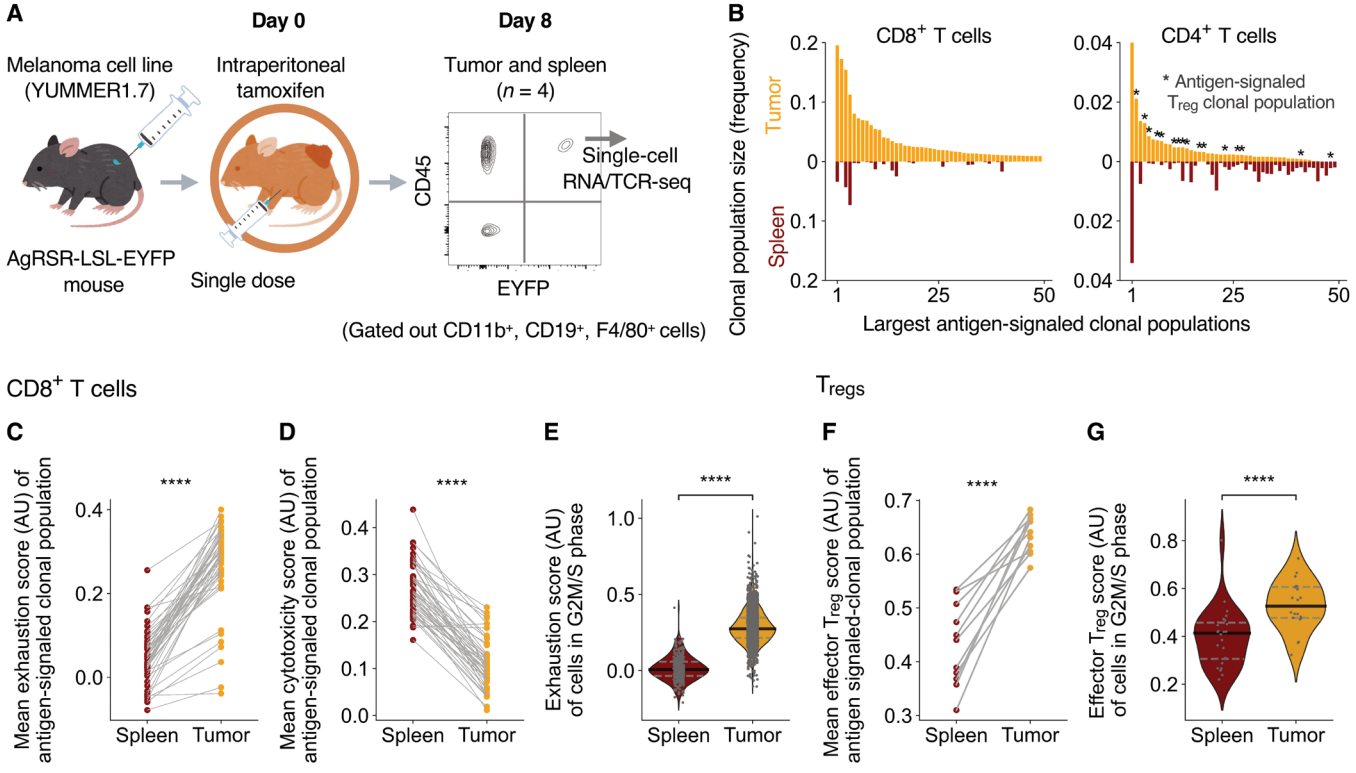

Fig. 3. Antigen-signaled CD8$^+$ T and T_{reg} cells partition their differentiation state by tissue site. (**A**) EYFP$^+$ T cells were sorted from tumors and spleens of AgRSR-LSL-EYFP mice 8 days after intraperitoneal tamoxifen injection and subjected to single-cell RNA and VDJ analysis ($n = 4$). (**B**) Largest antigen-signaled T cell clonal populations ranked by size, displaying clonal population sizes (frequencies) within tumors or spleens. (**C** to **G**) Antigen-signaled CD8$^+$ T cell (C to E) and T_{reg} (F and G) clonal populations with at least two cell members in both tumors and spleens assessed for mean exhaustion (C), cytotoxicity (D), and effector T_{reg} gene set expression score (F) in each tissue. Scores from the same antigen-signaled clonal population are linked by a line. (E and G) Violin plot comparing the gene set scores of individual cells in the G2M/S phase across tissues. Dots represent cells (E and G) and antigen-signaled clonal populations (C, D, and F). Statistical testing via paired two-tailed Student's *t* test and Kruskal-Wallis test (****$P < 0.0001$). AU, arbitrary units.

populations, antigen-signaled T_{reg} clonal populations distributed across spleens and tumors, on average, had higher effector T_{reg} scores in tumors than in spleens (Fig. 3F). Cells in a cycling phase in tumors had higher effector T_{reg} scores than equivalent cells in spleens (Fig. 3G).

Intratumoral antigen signals trap CD8$^+$ T cells in the tumor

We queried how CD8$^+$ T cells confine their exhausted state to the tumor site. Researchers using the Kaede system, which tracks the migration of all photoconverted CD8$^+$ T cells, have demonstrated egress of tumor T cells (including activated, antigen-specific CD8$^+$ T cells) to the lymphoid system (*8*, *9*, *35*), consistent with views that effector CD8$^+$ T cells reenter the recirculating immune system (*36*, *37*). To investigate the effect of intratumoral antigen signaling on CD8$^+$ T cell responses, we implanted congenic marker mice with B16-OVA melanoma tumors and injected activated TCR transgenic OT-I CD8$^+$ AgRSR-LSL-EYFP cells specific for the SIINFEKL peptide in OVA (Fig. 4A). Mice were then treated intratumorally with tamoxifen, which labels antigen-signaled T cells in the tumor (fig. S6, A to C). After 8 days, despite OT-I CD8$^+$ T cells being detected in both the tumor and the lymphoid tissues (Fig. 4B), EYFP$^+$ cells were detected almost exclusively in the tumors (Fig. 4C). The OVA/OT-I system models an exceptionally high, single antigen-TCR interaction. We therefore used the AgRSR system to investigate the effect of intratumoral signaling in a system for which a normal T cell repertoire can be activated by diverse neoantigens. YUMMER1.7-implanted AgRSR-LSL-EYFP mice were intratumorally injected with tamoxifen, and all CD8$^+$ EYFP$^+$ and a proportion of the CD8$^+$ EYFP$^-$ cells from the tumors and lymph nodes were processed through bulk TCR-seq 8 days after intratumoral tamoxifen administration (Fig. 4D). Again, EYFP$^+$

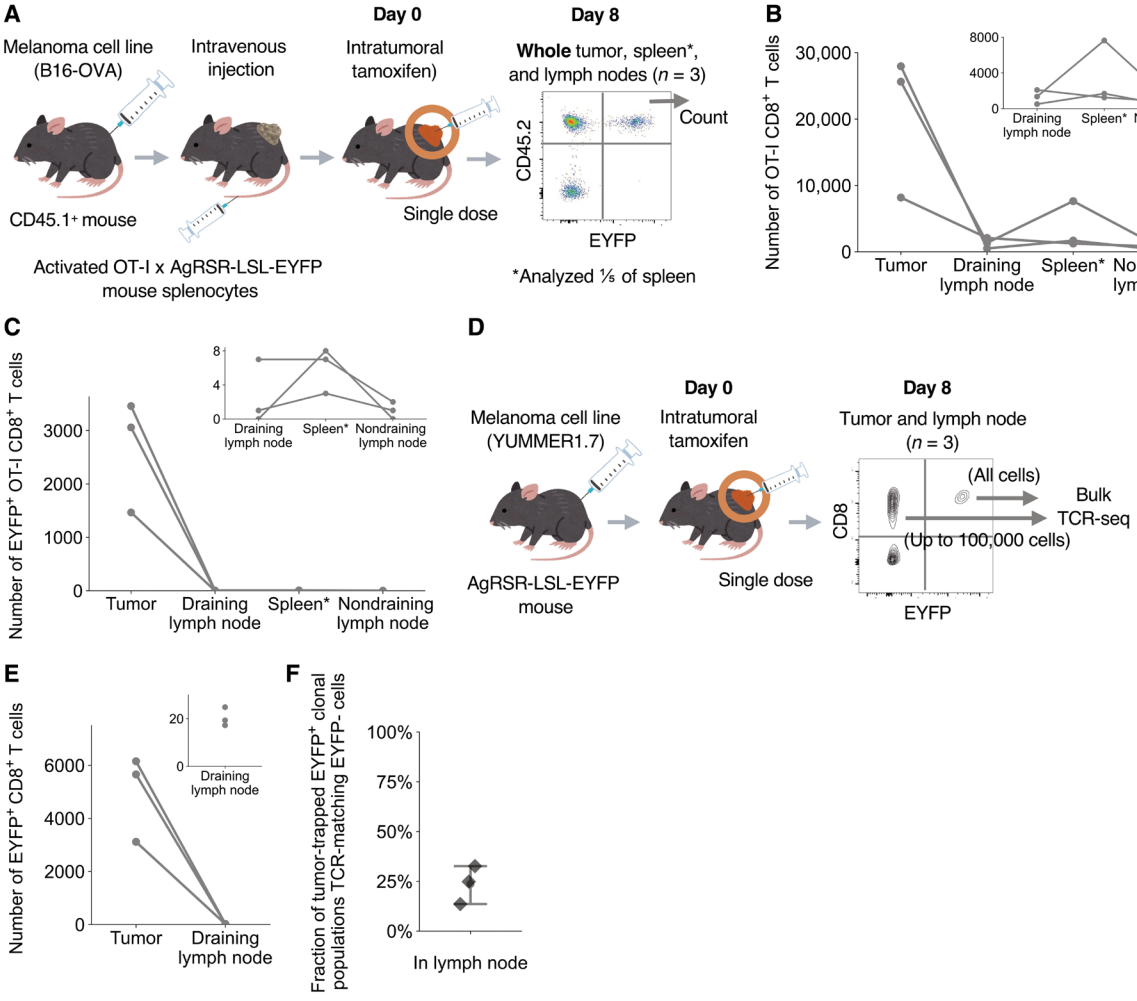

Fig. 4. Intratumoral antigen signaling traps CD8$^+$ T cells. (**A**) OT-I CD8$^+$ T cells from the whole tumors, draining and nondraining lymph nodes, and one-fifth of the spleens were analyzed 8 days after intratumoral tamoxifen administration of B16-OVA bearing congenic marker mice that had been injected with activated OT-I × AgRSR-LSL-EYFP mice 4 days earlier ($n = 3$). (**B** and **C**) Distribution of OT-I CD8$^+$ T cells (B) and EYFP$^+$ OT-I CD8$^+$ T cells (C) across different tissues with an enlarged view of lymphoid tissues (top right of respective figures). The asterisk denotes that one-fifth of the spleen was sampled. (**D**) EYFP$^+$ and EYFP$^-$ CD8$^+$ T cells were sorted from the tumor and draining lymph node of AgRSR-LSL-EYFP mice 8 days after intratumoral tamoxifen injection and subject to bulk TCR-seq analysis ($n = 3$). The top 200 largest EYFP$^+$ CD8$^+$ T cell clonal populations in the tumor of each mouse were analyzed. (**E**) Distribution of cells across the tumors and draining lymph nodes, with an enlarged view of the draining lymph nodes (top right). (**F**) Fraction of EYFP$^+$ clonal populations detected exclusively in tumors that had TCR overlap with EYFP$^-$ cells in draining lymph nodes. Dots represent mice (B, C, E, and F).

cells were detected almost exclusively in the tumors (Fig. 4E). Despite limited sampling of the EYFP$^-$ cells, a large fraction of clonal populations had overlapping TCRs with EYFP$^-$ cells in the lymph nodes (Fig. 4F). Together, these data demonstrate that intratumorally antigen-signaled CD8$^+$ T cell clonal populations become trapped in the tumor, even while cells from the same clonotype reside outside the tumor.

To investigate the transcriptomic characteristics of intratumorally antigen-signaled T cells, we analyzed sorted EYFP$^+$ T cells from tumors and spleens in three mice, 8 days after intratumoral injection, by paired scRNA-seq and TCR-seq (Fig. 5A). Both antigen-signaled CD8$^+$ and CD4$^+$ T cell clonal populations were substantially expanded in the tumors (Fig. 5B). In this experiment, EYFP$^+$ cells were sorted from whole spleens and tumors after magnetic bead enrichment for T cells. Consistent with our previous findings, cells of almost all antigen-signaled CD8$^+$ T cell clonal populations were trapped and confined to the tumors (Fig. 5, C and D). Tissue-trapping of activated T cells was not an artifact of the system because T_{reg} clones were readily detected in the spleen and tumor compartments (Fig. 5, C and D). We assessed whether tissue-trapped clonal populations were labeled after intraperitoneal tamoxifen. Half of the identified CD8$^+$ T cell clones were confined to the tumors, whereas more antigen-signaled T_{reg} clonal populations were distributed across both compartments (fig. S7A). Both fate-mapping strategies revealed antigen-signaled CD8$^+$ T cell clonal populations to be proliferating (fig. S7, B and D), to contain a subset of *Tcf7*-expressing stem cell–like cells with a capacity for self-renewal (fig. S7, C and E) (*38*), and to be exhausted in the tumor (Fig. 5E). We investigated how T_{reg} states change after intratumoral antigen signaling. The effector T_{reg} score decreased as cells left the tumor (Fig. 5F). Together, these data show that intratumoral antigen signaling generates tissue-trapped, exhausted, expanded, proliferating, and self-renewing CD8$^+$ T cell clonal populations in tumors.

Clustering time-stamped pseudo-time trajectories with TrajClust reveals determinants of CD8$^+$ T cell clonal population differentiation

Last, we investigated the response of antigen-signaled T cell clonal populations over time. We undertook paired scRNA-seq and TCR-seq analysis of EYFP$^+$ T cells from tumors and spleens at day 18 after intraperitoneal tamoxifen treatment in three mice (Fig. 6A). For all T cells, most cells in the spleens remained nonexpanded, whereas most cells in the tumors were composed of expanded clonal populations (fig. S9A). Again, we focused on the largest, expanded antigen-signaled clonal populations (Fig. 6B). Combining this dataset with our previous intraperitoneal dataset produced an atlas containing antigen-signaled CD8$^+$ T cell clonal populations with diverse reactivities. First, we sought to categorize these clonal populations to define major classes of clone differentiation.

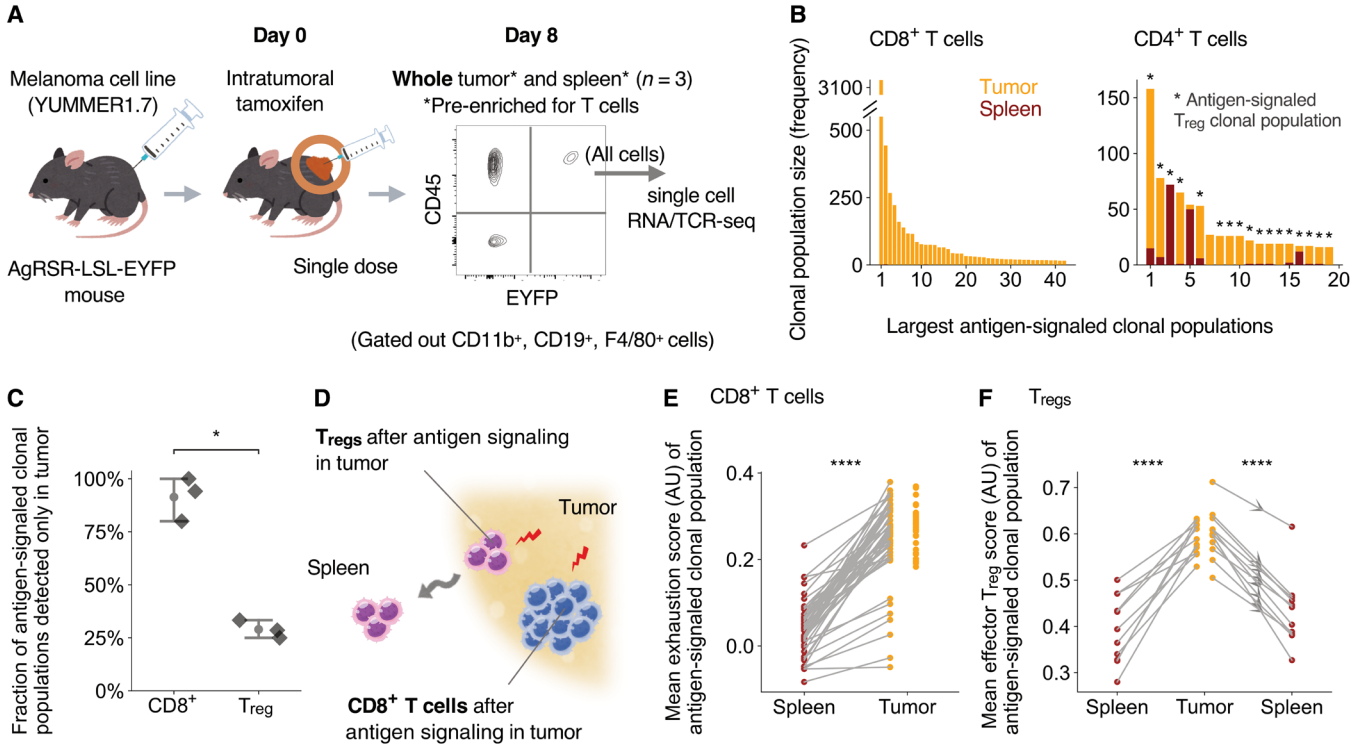

Fig. 5. Intratumoral antigen signals trap and exhaust CD8$^+$ T cells but not T_{regs}. (**A**) EYFP$^+$ T cells were sorted from whole preenriched tumors and spleens of AgRSR-LSL-EYFP mice 8 days after intratumoral tamoxifen injection and subject to single-cell RNA and VDJ analysis ($n = 3$). (**B**) Largest antigen-signaled T cell clonal populations ranked by size and colored by tissue origin. (**C**) Fraction of antigen-signaled CD8$^+$ T cell and T_{reg} clonal populations for which no cells with the same TCR were identified in EYFP$^+$ cells of the spleen. (**D**) Effect of intratumoral antigen signaling in CD8$^+$ T cell and T_{reg} clonal populations. (**E** and **F**) The average exhaustion and effector T_{reg} score of antigen-signaled CD8$^+$ T cell (E) and T_{reg} (F) clonal populations obtained from intraperitoneal fate-mapping (left section—as in Fig. 3, C and F) and intratumoral fate-mapping (right section and labeled with arrows for T_{reg} clonal populations). Dots represent antigen-signaled clonal populations (E and F) and mice (C). Statistical testing via paired two-tailed Student's *t* test and Kruskal-Wallis test (****$P < 0.0001$; *$P < 0.05$).

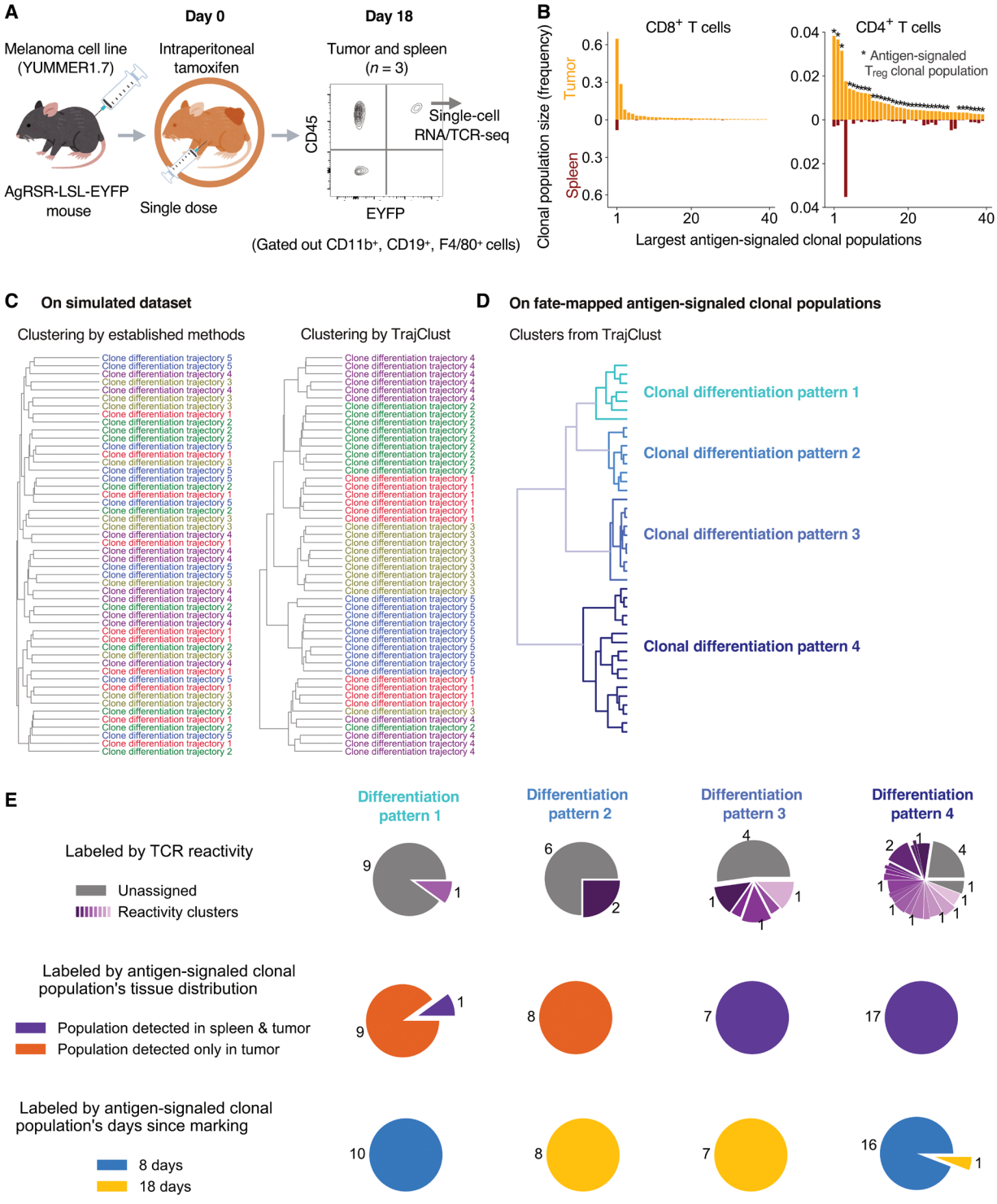

Fig. 6. Time elapsed since antigen signaling affects the differentiation state of CD8$^+$ T cells. (**A**) EYFP$^+$ T cells were sorted from tumors and spleens of AgRSR-LSL-EYFP mice 18 days after intraperitoneal tamoxifen injection and subject to single-cell RNA and VDJ analysis ($n = 3$). (**B**) Largest antigen-signaled T cell clonal populations ranked by size, displaying clonal population size (frequency) within tumors or spleens. (**C**) TrajClust, a computational algorithm to cluster clonal differentiation patterns, was applied to simulated datasets containing clonal populations with five different differentiation patterns. Results from an unsupervised clustering of these clonal populations by established methods (left) and TrajClust (right). (**D**) Unsupervised clustering of the largest antigen-signaled CD8$^+$ T cell clonal populations found 8 days (Fig. 3A) or 18 days (A) after intraperitoneal tamoxifen injection by TrajClust. Each cluster is denoted by clonal differentiation patterns 1 to 4. (**E**) Pie chart showing the properties of clonal populations from each clonal differentiation pattern. Clonal populations are labeled by their TCR reactivity groups identified by GLIPH2 analysis (top), their tissue distribution (middle), and their time elapsed since antigen signaling (bottom).

Established methods to compare clonal populations (*39*–*41*) base comparisons on differentiation state distributions that lose key information about the similarities between clonal populations. We therefore developed TrajClust, an algorithm to cluster clonal populations based on transcriptome-wide differentiation trajectory similarities (see the Supplementary Materials). Simulated datasets of distinct clone differentiation patterns demonstrated that TrajClust could successfully discover clusters of clonal differentiation patterns that an established clone clustering method using Uniform Manifold Approximation and Projection (UMAP)–based similarities could not (Fig. 6C and fig. S8, A to G). When TrajClust was applied to our atlas, four major clonal differentiation patterns were identified (Fig. 6D and fig. S8H), characterized by groups of differentially expressed genes in the tumor (data file S1). We queried whether reactivity to a specific antigen could account for these patterns using GLIPH2 (grouping of lymphocyte interactions by paratope hotspots) (*42*), an algorithm that identifies reactivity clusters within TCR sequences from multiple donors, but we found no single reactivity driving this clustering. The major clusters corresponded to the time since antigen signaling and the tissue confinement of the antigen-signaled clonal populations (Fig. 6E). These results therefore demonstrate that irrespective of reactivity, the differentiation of antigen-signaled clonal populations is consistent and is chiefly determined by the duration of their persistence.

Time elapsed since antigen signaling affects the tissue distribution of differentiated T cell clonal populations

These results raised the question of how functional states were affected by the duration of population persistence. Again, we filtered the $CD4^+$ T cell clonal populations by *Foxp3* expression. Both antigen-signaled $CD8^+$ T cell and T_{reg} clonal populations continued to express genes indicative of tissue-dependent differentiation, as observed at day 8 (fig. S9, B to E). We analyzed changes in the antigen-signaled $CD8^+$ T cell and T_{reg} clonal populations between days 8 and 18. In antigen-signaled $CD8^+$ T cell clonal populations, the fraction of cycling cells decreased, with almost no antigen-signaled clonal populations containing cycling cells in the spleens by day 18 (Fig. 7A). A lower fraction of cells from antigen-signaled $CD8^+$ T cell clonal populations was also found in the spleens

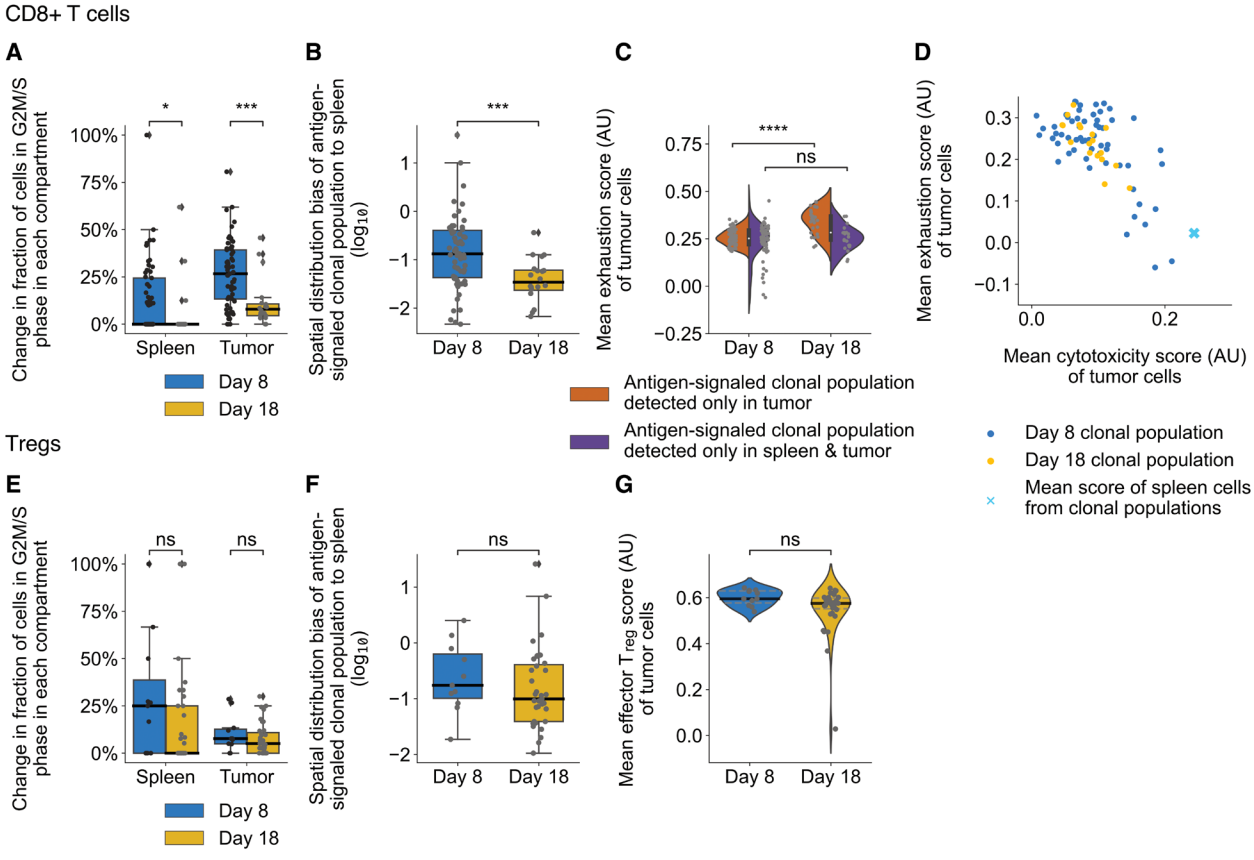

Fig. 7. Spatial distribution changes of antigen-signaled T cell clonal populations. (**A** to **G**) Tracking changes in antigen-signaled T cell clonal populations over days 8 and 18. (A and E) Changes in the fraction of cells in the G2M/S phase across tissues for antigen-signaled $CD8^+$ T cell (A) and T_{reg} (E) populations. (B and F) Changes in the spatial distribution bias of antigen-signaled $CD8^+$ T cell (B) and T_{reg} (F) clonal populations. The spatial distribution bias was calculated by dividing the clonal population size (frequency) in the spleen by that of the tumor. (C and G) Changes in the mean exhaustion and T_{reg} effector gene set score of tumor cells from antigen-signaled $CD8^+$ T cell (C) and T_{reg} (G) clonal populations. (D) Mean exhaustion and cytotoxic scores of antigen-signaled $CD8^+$ T cell clonal populations, restricted to analysis of their cells from tumors (small dots) or secondary lymphoid tissues (large cross—mean of all clonal populations). Individual clonal populations are colored by time elapsed since antigen signaling. Dots represent antigen-signaled clonal populations (A to G). Statistical testing via paired two-tailed Student's *t* test and Kruskal-Wallis test (****$P < 0.0001$; ***$P < 0.001$; *$P < 0.05$; ns, $P > 0.05$).

(Fig. 7B). We assessed changes in exhaustion and found this to significantly increase in antigen-signaled clonal populations found exclusively in the tumors (Fig. 7C and S9D). There was no significant change in the average exhaustion of clonal populations containing cells in both the lymphoid system and tumors. The overall exhaustion of some clonal populations was low at day 8, but no clones with low exhaustion were present at day 18. Because the level of cytotoxicity in cycling secondary lymphoid system cells remained constant (fig. S9F), we hypothesized that this would mean $CD8^+$ T cell clonal populations lose their influx of cytotoxic cells over time and become exhausted. Although some clonal populations within the tumors appeared cytotoxic and functional on day 8, these did not exist at the latter time point on day 18 (Fig. 7D). In antigen-signaled T_{reg} clonal populations, neither the fraction of cycling cells, the spatial distribution of the antigen-signaled clonal population, nor the effector T_{reg} score changed significantly between days 8 and 18 (Fig. 7, E to G).

DISCUSSION

In this study, we developed and validated a fate-mapping mouse to track lymphocytes based on antigen signaling. Our system enables the marking of lymphocytes that respond to antigen signals at different times and locations. We successfully validated the system's specificity for exclusively marking lymphocytes (and their progenies) that have received antigen signaling in vivo. We note that intratumoral tamoxifen injection may leak because a barely detectable number of $EYFP^+$ events were recorded from T cells taken from extratumoral sites (fig. S6, A to C). Any leakage would work against our findings by marking T cells as extratumorally activated, thus increasing the likelihood of detecting $EYFP^+$ cells in the lymphoid tissues, but we highlight the limitation of this injection method for potential users. Alongside the capacity for fate-mapping $CD8^+$ T cells, this system tracks (self-) antigen-stimulated conventional and T_{reg} $CD4^+$ T cells. These cell types maintain tissue homeostasis in response to pathogen, autoimmune, and sterile inflammatory challenges, and the application of this system could provide insights into myriad aspects of infection, autoimmunity, and cancer.

Using the AgRSR system, we report how intratumoral antigen signals act as gatekeepers to compartmentalize $CD8^+$ T cell responses. The antigen receptor of the $CD8^+$ T cell, the TCR, evaluates only antigenic structure to determine clone selection (*43*). It cannot, by itself, evaluate the pathogenicity of the antigenic source nor the load and distribution of the antigen. Sustained work over the past three decades has demonstrated how the former constraint is overcome by innate immune recognition signals, but no mechanism has been proposed to address the latter constraint, despite millennia of coevolution with pathogens necessitating a need to balance pathogen control with destructive immune responses. Our work suggests a mechanism by which tissue-specific antigen signaling confines $CD8^+$ T cell activity to a particular tissue niche. $CD8^+$ T cells are primed by an "initial" hit, whereas a "second" hit at the effector site both engages and commits a subset of these cells to the tissue niche. Through this "two-hit" mechanism, $CD8^+$ T cells that have engaged with antigen and become exhausted cannot compromise systemic protection. In the context of chronic pathogens, immunity could therefore separate its responses between tissues with insurmountably high antigenic load and tissues with surmountable antigenic load, enabling pathogen control to be balanced with organism survival.

MATERIALS AND METHODS

Study design

The objective of this study was to investigate the effect of antigen signaling on T cell responses. We developed a reporter mouse and applied it to a murine tumor model to compare responses of T cells receiving antigen signals systemically and intratumorally. All mouse experiments were performed with random assignment of mice without investigator blinding, with at least two biological replicates per experimental group. All data describe biological replicates unless otherwise stated.

BAC clone modification and purification

A bacterial artificial chromosome (BAC) clone containing the *Nr4a1* gene (BACPAC resources) was modified by introducing Katushka E2A–linked CreERT2-SV40 polyadenylation signal into the start ATG of the *Nur77* gene by homologous recombination (*44*). BAC DNA was purified from 200 ml of bacterial cultures by alkaline lysis (Qiagen buffers), and circular DNA was separated by CsCl ultracentrifugation. Briefly, 4.04 g of CsCl was added to 4 ml of resuspended DNA, and CsCl was dissolved at 40°C. Twenty-five microliters of EtBr (10 mg/ml) and 75 μl of water were added. Samples were spun in a bench tube centrifuge at 3000 rpm for 15 min to remove the remaining proteins. The DNA CsCl solution was spun at 70,000*g* for 6 hours. EtBr was removed by *n*-butanol extraction, and the DNA was precipitated. Successful recombination was confirmed by polymerase chain reaction (PCR). The DNA was spot-dialyzed on Millipore VSWPO2500 filters into polyamine buffer [10 mM tris-Cl (pH 7.5), 0.1 mM EDTA, 100 mM NaCl, 30 μM spermine, and 70 μM spermidine].

Experimental mice

AgRSR mice were generated via pronuclear injection of the modified BAC DNA into 0.5-day-fertilized ova of C57BL/6 donors. Founder lines were assessed for transgene expression, and the line with the highest expression was crossed with the ROSA26-LSL-EYFP mice (gift from D. Winton, CRUK-CI, Cambridge). The AgRSR, AgRSR-LSL-EYFP, OT-I × AgRSR-LSL-EYFP, $B2m^{-/-}$ (Jax, 002087), and $RAG2^{-/-}$ (Jax, 008449) mice were maintained in CRUK Cambridge Institute Biological Resources Unit and University of Cambridge Central Biomedical Service under specific pathogen–free conditions. All animal experiments were conducted when mice were between 8 and 12 weeks of age and were conducted in accordance with Home Office guidelines.

Listeria, vaccine, and tumor challenges

Mice were infected with 1500 colony-forming units of *Listeria monocytogenes* in experiments indicated in the text. For immunization, mice were intraperitoneally injected with 50 μg of SIINFEKL peptide, 10 μg of anti-CD40 (Bio X cell), and 10 μg of poly(I:C) (InvivoGen). For the generation of murine tumors, cells of the cultured YUMMER1.7 cell line (*23*) (a gift from M. Bosenberg) or the B16-OVA cell line (*45*) (a gift from R. Roychoudhuri) were detached with 0.5% trypsin-EDTA (Gibco) for 3 min, quenched with complete media, and washed in phosphate-buffered saline (PBS) three times. Single-cell suspensions of 1 million cells (YUMMER1.7) or 200,000

cells (B16-OVA) were subcutaneously injected into the right flank of each mouse. In vivo tumor volumes were monitored by (width × depth × length)/2 using a caliper.

Tamoxifen administration

Tamoxifen (20 mg/ml) was prepared in ethanol (5% v/v) and sunflower oil (95% v/v) before dissolving in a 37°C water bath under sonication (35 kHz) for 15 min. Tamoxifen (2 mg) was administered by intraperitoneal injection 24 hours after the *Listeria* challenges, at 0 and 12 hours after the vaccine challenges, 5 days before tumor implantation in the tamoxifen pretumor challenge, or at day 7 after subcutaneous tumor implantation in all other tumor experiments. For fate-mapping antigen signaling within the tumors, 10 μl of 4-hydroxytamoxifen (4OHT) at 39 mg/ml was injected into tumors on day 10 after subcutaneous tumor injection.

Generation of single-cell suspensions from tissues

Lymph nodes and spleens were homogenized in PBS/0.1% fetal calf serum (FCS)/2 mM EDTA and filtered (70- or 100-μm filters). Red blood cell lysis buffer ($NH_4Cl/NaHCO_3$/EDTA) was used to lyse splenic erythrocytes. Tumors were cut into pieces by a scissor and digested using the Miltenyi Tumor Dissociation Kit, according to the manufacturer's instructions, before filtering (100 then 70 μm) to generate a single-cell suspension.

Culturing T cells

Purified T cells from spleens and, where applicable, from tumors and draining and nondraining lymph nodes were cultured in complete RPMI 1640 (10% fetal bovine serum and 55 mM 2-mercaptoethanol). Media were supplemented with interleukin-2 (IL-2; 20 ng/ml), IL-7 (2 ng/ml), the SIINFEKL peptide, and its variants at (5 μg/ml) and incubated at 37°C and 5% CO_2 for 24 hours to check for Katushka expression or for 72 hours to check for EYFP expression.

Flow cytometry

Surface antibody staining was performed by incubating cells with antibodies against CD3 (17A2: BV421 and PE-Cy7, BioLegend), CD3e (45-2C11: FITC, eBioscience; 145-2C11: APC/Fire750, BioLegend), CD4 (RM4-5: BV650 and BV785, BioLegend; GK1.5: BV605, BioLegend), Cd8a (53-6.7: APC and BV650, BioLegend), CD11b (M1/70: BV510, PE/Cy7, and APC/Fire750, BioLegend), CD19 (6D5: BV510 and PE/Cy7, BioLegend), CD44 (IM7: PE and APC/Fire750, BioLegend), CD45 (30-F11: APC, eBioscience; 30-F11: BV785, BioLegend), CD45.1 (A20: PE, BioLegend), CD45.2 (104: BV786, BD Horizons), CD62L (MEL-14: BV421 and APC, BioLegend), CD69 (H1.2F3: APC/Fire750, BioLegend), F4/80 (BM8: PE/Cy7, BioLegend), CD279 (29F.1A12: BV421, BioLegend), NK1.1 (S17016D: PE/Cy7, BioLegend), and Ter^{119} (TER^{119}: PE/Cy7, BioLegend). Staining was conducted in PBS containing 0.1% FCS and 2 mM EDTA for 30 min at 4°C to cells that had been preincubated with TruStain FcX (anti-mouse CD16/32). This was preceded by LIVE/DEAD Fixable Aqua or Blue (Invitrogen) staining in PBS (1:100) for 10 min at room temperature for dead cell exclusion. Samples were fixed by incubating in a buffer containing 1% formaldehyde/0.02% sodium azide/glucose/PBS for 10 min at room temperature. Data were acquired on an LSR Fortessa (BD Bioscience) flow cytometer and further analyzed by Flowjo v10 (Treestar). Example gating strategies are shown (fig. S10).

Preparation of cells for bulk TCR-seq and single-cell RNA/TCR-seq

Cell suspensions from the tumor, spleen, and draining and nondraining lymph nodes were generated independently. Samples were stained for fluorescence-activated cell sorting (FACS) analysis for 30 min on ice. Live immune cells were sorted using a FACSAria instrument (BD Bioscience) with a 100-μm nozzle. For bulk TCR-seq, T cells were preenriched from spleen single-cell suspensions by magnetic bead purification using Miltenyi beads. The whole tissue was sorted to capture all $EYFP^+$ and 100,000 $EYFP^-$ $CD8^+$ T cells from each sample. Sorted cells were collected in Buffer RLT Plus (Qiagen) with 20 mM dithiothreitol. Lysate was vortexed for 1 min and stored at −80°C for subsequent analysis. For scRNA-seq/TCR-seq, cells were sorted into PBS containing 10% FCS and 2 mM EDTA in cold and spun down at 300*g* 7 min 4°C before resuspension in PBS to achieve a final concentration of 10,000 to 20,000 cells/32 μl. Totalseq C Hashtag antibodies were added to individual tissues at 0.1 mg/ml before scRNA-seq/TCR-seq to barcode spleen samples to enable pooled library preparation; cells were then washed twice and sorted. In the intratumoral injection experiment, T cells were preenriched from tumor and spleen single-cell suspensions by magnetic bead purification, and the whole sample was sorted.

scRNA/TCR-seq analysis

scRNA-seq libraries were prepared using Chromium Single Cell and V(D)J Enrichment Kits following the Single-Cell V(D)J Reagent Kits User Guide (Manual Part CG000086 Rev. H, I, J, K, L, M; 10x Genomics). The data from the experiment using intraperitoneal tamoxifen were generated using chemistry (5′ v 1) before the introduction of the dual-indexing strategy; the data for the intratumoral 4OHT experiment were generated using chemistry (5′ v 2). Sorted samples were resuspended in PBS and 0.04% BSA and loaded into Chromium microfluidic chips to generate single-cell gel-bead emulsions using the Chromium controller (10x Genomics). RNA from the barcoded cells for each sample was reverse-transcribed in a C1000 Touch Thermal cycler (Bio-Rad), and libraries were generated according to the manufacturer's protocol with no modifications (14 cycles used for cDNA amplification). For single-cell libraries, samples were sequenced on an Illumina HiSeq 4000 as 2× 150 paired-end reads, one full lane per pool [before analysis, gene expression data were trimmed to 26 base pairs (bp), read 1; 8 bp, i7 index; and 98 bp, read 2] or run on Illumina NovaSeq6000 with the same parameters (PE150, gene expression libraries trimmed to 28:8:0:98). Gene expression raw sequencing data were processed using CellRanger software v.3.0, and the TCR alpha and beta chains were processed using CellRanger VDJ v.3.1.0, both following the CellRanger pipeline. Sequencing reads were aligned to the mouse reference genome mm10 (Ensembl 93) provided by CellRanger.

Bulk TCR β analysis

Total RNA was isolated with RNeasy Micro Kit (Qiagen) according to the manufacturer's protocol and increasing RNA elution time to 10 min. Libraries were prepared using SMARTer Mouse TCR α/β Profiling kit (Takara Bio USA) following recommendations for 10 to 100 ng of purified total RNA input and using primers for both α and β TCR chains. Final clean-up was performed with SPRIselect reagent (Beckman Coulter). Pooled libraries were sequenced with Illumina NextSeq 2000 P2 600 cycles kit 300PE with the 10% PhiX. Sequencing data were analyzed and clonal populations were identified using

MiXCR v4.4.2 (*46*) with recommended settings for SMARTer Mouse TCR α/β Profiling kit (analyze takara-mouse-rna-tcr-smarter). Cells were grouped by their TCR β sequences, and the top 200 largest $EYFP^+$ clonal populations (by frequency in the tumor) from each mouse were used for subsequent analysis. Sequences matching public repertoires were removed (Immune Epitope Database).

Adoptive transfer

To determine the duration of tamoxifen activity, splenocytes were stimulated with anti-CD3 (2 μg/ml) and anti-CD28 (10 μg/ml) for 24 hours and intravenously transferred (3×10^6 cells per mouse) into CD45.1 $RAG2KO^{-/-}$ mice. In the B16-OVA experiment, $CD44+ CD8^+$ T cells (1×10^6 per mouse) from OT-I × AgRSR-LSL-EYFP mice were intravenously transferred into B16-OVA-bearing mice, 10 days after tumor inoculation following published protocols (*8*).

Processing of antigen-signaled T cell clonal populations

From the scRNA/TCR-seq data, cells expressing identical TCR alpha and beta [V(D)J] nucleotide sequences were defined as antigen-signaled T cell clonal populations. Antigen-signaled T cell clonal populations were classified as antigen-signaled $CD8^+$ or $CD4^+$ T cell clonal populations if more than 60% of cells or fewer than 60% of cells in the population expressed *Cd8a*, respectively. Antigen-signaled T_{reg} clonal populations were computationally defined as antigen-signaled $CD4^+$ T cell clonal populations in which more than 10% of cells expressed *Foxp3*. Downstream analysis was restricted to cells from spleens and tumors, clonal populations of sizes greater than 15 with cells in tumors, and, in the case of the intratumoral dataset, clonal populations from mice that had no evidence of tamoxifen leakage. Clonal population size (frequency) was calculated as the number of cells in the spleen and tumor of each clonal population as a fraction of the total captured T cells in the tissue compartment.

Gene set scores

The gene sets for cell cycle status were taken from Tirosh *et al.* (*29*), and the CellCycleScoring module was used to assign cells either a G1 or G2M/S phase (proliferating) status in Seurat. Gene sets from Li *et al.* (*28*), Bending *et al.* (*34*), and Yost *et al.* (2019) (*47*) [based on (*38*)] were used to score cells for exhaustion, effector T_{reg} differentiation, and Tcf7 self-renewal capacity, respectively. Additional gene sets from Lucca *et al.* (*30*), Wherry *et al.* (*32*), and Beltra *et al.* (*48*) [based on (*31*)] were used to corroborate results from the exhaustion score analysis. Mouse ortholog genes (*49*) (based on Ensembl Biomart version 87) were used when gene sets were derived from human data. Gene set scores were calculated by normalizing and taking the log of the raw gene counts obtained from the CellRanger output and applying the score_genes function from Scanpy with the required gene set, as in (*29*). Scores were produced for each cell, and these were then averaged across cell members of a clonal population (or other subsets of cells as indicated in the text) to calculate scores for each clonal population.

Human data

Data from Gueguen *et al.* (*33*) were downloaded from GSE162498 and reprocessed using the same analysis pipeline.

Integrating the scRNA/TCR-seq data for clustering and pseudo-time analysis

To prevent the variable TCR genes from contributing to downstream analysis, genes containing TRAV and TRBV in their gene name were removed from the gene-expression matrix. The resulting count matrices and V(D)J sequences were further processed using scRepertoire (*50*), Seurat (*51*), and Scanpy (*52*). Briefly, the samples were demultiplexed with the aid of the HTODemux function, matched to their V(D)J sequences with the combineTCR and combineExpression functions, filtered [to cells that had full TCR alpha and beta (V(D)J) nucleotide sequences, feature counts in the 200-to-5000 range, and less than 10% mitochondrial counts], preprocessed by the SCTransform function, and integrated with the FindIntegrationAnchors and IntegrateData functions (*53*). Relevant cells were subset from the main dataset, and principal components analysis (number of dimensions = 50) and UMAP coordinates were generated for Louvain clustering (*54*, *55*) (resolution = 1.5) and Monocle 3 (*56*) pseudo-time analysis.

TrajClust algorithm

TrajClust was evaluated on simulated datasets to demonstrate that it could reveal shared differentiation patterns that would have otherwise been hidden (further details are in "Development and testing of TrajClust" in the Supplementary Materials). TrajClust was applied to clonal populations from days 8 and 18 intraperitoneal tamoxifen datasets, restricted to those of size 75 or greater. One clonal population with a distinct differentiation state was considered an outlier and removed from the dataset before analysis. The hierarchical clustering results were flattened to discrete clusters by choosing the cluster size that maximized the silhouette score of the resulting clusters. This resulted in four clusters denoted clonal differentiation patterns.

GLIPH2 analysis

GLIPH2 (*42*) using CDR3a, CDR3b, TRBV, and TRAJ sequences was applied to all clonal populations of size greater than 15 from days 8 and 18 intraperitoneal tamoxifen datasets to uncover common reactivity groups. Some clonal populations were assigned to multiple reactivity groups. This was represented in Fig. 6E by equally dividing a clonal population's allocation in the pie chart into their respective reactivity groups.

Software versions

Data were analyzed using R version 4.0.3 and R packages (Seurat 4.0.4, SeuratData 0.2.1, SeuratDisk 0.0.0, scRepertoire 1.0.0, splatter 1.14.1, and monocle3 0.2.3), as well as Python version 3.8.6 and Python packages (jupyterlab 2.2.9, numpy 1.19.4, pandas 1.1.5, scipy 1.6.0, scanpy 1.6.0, anndata 0.7.5, rpy2 3.3.6, anndata2ri 1.0.5.dev2 + ea266ab, skmisc 0.1.3, sktime 0.5.2, scikit-learn 0.24.1, and tqdm 4.54.1). Figures were produced with seaborn 0.11.0, matplotlib 3.5.1 in Python, GraphPad Prism 10, Affinity Publisher 1.10.8, and using illustrations from Irasutoya (www.irasutoya.com/).

Statistical analysis

Statistical analyses on the FACS data were performed using two-tailed Student's *t* tests unless otherwise indicated. Differentially expressed genes were recorded for genes with $P < 0.01$ and $\log_2 F > 0.5$. Paired comparisons were assessed for statistical significance using Kruskal-Wallis with Scipy.

Supplementary Materials

This PDF file includes:

Supplementary Text
Figs. S1 to S10
References (*58*–*66*)

Other Supplementary Material for this manuscript includes the following:
Data Files S1 and S2
MDAR Reproducibility Checklist

REFERENCES AND NOTES

1. D. R. Sen, J. Kaminski, R. A. Barnitz, M. Kurachi, U. Gerdemann, K. B. Yates, H. W. Tsao, J. Godec, M. W. LaFleur, F. D. Brown, P. Tonnerre, R. T. Chung, D. C. Tully, T. M. Allen, N. Frahm, G. M. Lauer, E. J. Wherry, N. Yosef, W. N. Haining, The epigenetic landscape of T cell exhaustion. *Science* **354**, 1165–1169 (2016).
2. K. E. Pauken, M. A. Sammons, P. M. Odorizzi, S. Manne, J. Godec, O. Khan, A. M. Drake, Z. Chen, D. R. Sen, M. Kurachi, R. A. Barnitz, C. Bartman, B. Bengsch, A. C. Huang, J. M. Schenkel, G. Vahedi, W. N. Haining, S. L. Berger, E. J. Wherry, Epigenetic stability of exhausted T cells limits durability of reinvigoration by PD-1 blockade. *Science* **354**, 1160–1165 (2016).
3. A. Schietinger, M. Philip, V. E. Krisnawan, E. Y. Chiu, J. J. Delrow, R. S. Basom, P. Lauer, D. G. Brockstedt, S. E. Knoblaugh, G. J. Hämmerling, T. D. Schell, N. Garbi, P. D. Greenberg, Tumor-specific T cell dysfunction is a dynamic antigen-driven differentiation program initiated early during tumorigenesis. *Immunity* **45**, 389–401 (2016).
4. M. A. ElTanbouly, R. J. Noelle, Rethinking peripheral T cell tolerance: Checkpoints across a T cell's journey. *Nat. Rev. Immunol.* **21**, 257–267 (2021).
5. A. Schietinger, P. D. Greenberg, Tolerance and exhaustion: Defining mechanisms of T cell dysfunction. *Trends Immunol.* **35**, 51–60 (2014).
6. S. J. Im, B. T. Konieczny, W. H. Hudson, D. Masopust, R. Ahmed, PD-1+ stemlike CD8 T cells are resident in lymphoid tissues during persistent LCMV infection. *Proc. Natl. Acad. Sci. U.S.A.* **117**, 4292–4299 (2020).
7. N. V. Gavil, M. C. Scott, E. Weyu, O. C. Smith, S. D. O'Flanagan, S. Wijeyesinghe, S. Lotfi-Emran, S. L. Shiao, V. Vezys, D. Masopust, Chronic antigen in solid tumors drives a distinct program of T cell residence. *Sci. Immunol.* **8**, eadd5976 (2023).
8. Z. Li, Z. K. Tuong, I. Dean, C. Willis, F. Gaspal, R. Fiancette, S. Idris, B. Kennedy, J. R. Ferdinand, A. Peñalver, M. Cabantous, S. Murtuza Baker, J. W. Fry, G. Carlesso, S. A. Hammond, S. J. Dovedi, M. R. Hepworth, M. R. Clatworthy, D. R. Withers, In vivo labeling reveals continuous trafficking of TCF-1+ T cells between tumor and lymphoid tissue. *J. Exp. Med.* **219**, e20210749 (2022).
9. M. M. Steele, A. Jaiswal, I. Delclaux, I. D. Dryg, D. Murugan, J. Femel, S. Son, H. du Bois, C. Hill, S. A. Leachman, Y. H. Chang, L. M. Coussens, N. Anandasabapathy, A. W. Lund, T cell egress via lymphatic vessels is tuned by antigen encounter and limits tumor control. *Nat. Immunol.* **24**, 664–675 (2023).
10. F. Djenidi, J. Adam, A. Goubar, A. Durgeau, G. Meurice, V. de Montpréville, P. Validire, B. Besse, F. Mami-Chouaib, CD8+CD103+ tumor-infiltrating lymphocytes are tumor-specific tissue-resident memory T cells and a prognostic factor for survival in lung cancer patients. *J. Immunol.* **194**, 3475–3486 (2015).
11. T. Duhen, R. Duhen, R. Montler, J. Moses, T. Moudgil, N. F. de Miranda, C. P. Goodall, T. C. Blair, B. A. Fox, J. E. McDermott, S. C. Chang, G. Grunkemeier, R. Leidner, R. B. Bell, A. D. Weinberg, Co-expression of CD39 and CD103 identifies tumor-reactive CD8 T cells in human solid tumors. *Nat. Commun.* **9**, 2724 (2018).
12. G. Oliveira, K. Stromhaug, S. Klaeger, T. Kula, D. T. Frederick, P. M. le, J. Forman, T. Huang, S. Li, W. Zhang, Q. Xu, N. Cieri, K. R. Clauser, S. A. Shukla, D. Neuberg, S. Justesen, G. MacBeath, S. A. Carr, E. F. Fritsch, N. Hacohen, M. Sade-Feldman, K. J. Livak, G. M. Boland, P. A. Ott, D. B. Keskin, C. J. Wu, Phenotype, specificity and avidity of antitumour CD8(+) T cells in melanoma. *Nature* **596**, 119–125 (2021).
13. C. S. Eberhardt, H. T. Kissick, M. R. Patel, M. A. Cardenas, N. Prokhnevska, R. C. Obeng, T. H. Nasti, C. C. Griffith, S. J. Im, X. Wang, D. M. Shin, M. Carrington, Z. G. Chen, J. Sidney, A. Sette, N. F. Saba, A. Wieland, R. Ahmed, Functional HPV-specific PD-1(+) stem-like CD8 T cells in head and neck cancer. *Nature* **597**, 279–284 (2021).
14. E. R. Kearney, K. A. Pape, D. Y. Loh, M. K. Jenkins, Visualization of peptide-specific T cell immunity and peripheral tolerance induction in vivo. *Immunity* **1**, 327–339 (1994).
15. T. A. Shih, M. Roederer, M. C. Nussenzweig, Role of antigen receptor affinity in T cell-independent antibody responses in vivo. *Nat. Immunol.* **3**, 399–406 (2002).
16. T. G. Phan, M. Amesbury, S. Gardam, J. Crosbie, J. Hasbold, P. D. Hodgkin, A. Basten, R. Brink, B cell receptor-independent stimuli trigger immunoglobulin (Ig) class switch recombination and production of IgG autoantibodies by anergic self-reactive B cells. *J. Exp. Med.* **197**, 845–860 (2003).
17. J. J. Taylor, R. J. Martinez, P. J. Titcombe, L. O. Barsness, S. R. Thomas, N. Zhang, S. D. Katzman, M. K. Jenkins, D. L. Mueller, Deletion and anergy of polyclonal B cells specific for ubiquitous membrane-bound self-antigen. *J. Exp. Med.* **209**, 2065–2077 (2012).
18. J. D. Altman, P. A. H. Moss, P. J. R. Goulder, D. H. Barouch, M. G. McHeyzer-Williams, J. I. Bell, A. J. McMichael, M. M. Davis, Phenotypic analysis of antigen-specific T lymphocytes. *Science* **274**, 94–96 (1996).
19. A. E. Moran, K. L. Holzapfel, Y. Xing, N. R. Cunningham, J. S. Maltzman, J. Punt, K. A. Hogquist, T cell receptor signal strength in T_{reg} and iNKT cell development demonstrated by a novel fluorescent reporter mouse. *J. Exp. Med.* **208**, 1279–1289 (2011).
20. J. Zikherman, R. Parameswaran, A. Weiss, Endogenous antigen tunes the responsiveness of naive B cells but not T cells. *Nature* **489**, 160–164 (2012).
21. K. A. Hogquist, S. C. Jameson, W. R. Heath, J. L. Howard, M. J. Bevan, F. R. Carbone, T cell receptor antagonist peptides induce positive selection. *Cell* **76**, 17–27 (1994).
22. C. H. Wilson, I. Gamper, A. Perfetto, J. Auw, T. D. Littlewood, G. I. Evan, The kinetics of ER fusion protein activation in vivo. *Oncogene* **33**, 4877–4880 (2014).
23. J. Wang, C. J. Perry, K. Meeth, D. Thakral, W. Damsky, G. Micevic, S. Kaech, K. Blenman, M. Bosenberg, UV-induced somatic mutations elicit a functional T cell response in the YUMMER1.7 mouse melanoma model. *Pigment Cell Melanoma Res.* **30**, 428–435 (2017).
24. C. J. Perry, A. R. Muñoz-Rojas, K. M. Meeth, L. N. Kellman, R. A. Amezquita, D. Thakral, V. Y. du, J. X. Wang, W. Damsky, A. L. Kuhlmann, J. W. Sher, M. Bosenberg, K. Miller-Jensen, S. M. Kaech, Myeloid-targeted immunotherapies act in synergy to induce inflammation and antitumor immunity. *J. Exp. Med.* **215**, 877–893 (2018).
25. E. Song, T. Mao, H. Dong, L. S. B. Boisserand, S. Antila, M. Bosenberg, K. Alitalo, J. L. Thomas, A. Iwasaki, VEGF-C-driven lymphatic drainage enables immunosurveillance of brain tumours. *Nature* **577**, 689–694 (2020).
26. A. C. Huang, M. A. Postow, R. J. Orlowski, R. Mick, B. Bengsch, S. Manne, W. Xu, S. Harmon, J. R. Giles, B. Wenz, M. Adamow, D. Kuk, K. S. Panageas, C. Carrera, P. Wong, F. Quagliarello, B. Wubbenhorst, K. D'Andrea, K. E. Pauken, R. S. Herati, R. P. Staupe, J. M. Schenkel, S. McGettigan, S. Kothari, S. M. George, R. H. Vonderheide, R. K. Amaravadi, G. C. Karakousis, L. M. Schuchter, X. Xu, K. L. Nathanson, J. D. Wolchok, T. C. Gangadhar, E. J. Wherry, T-cell invigoration to tumour burden ratio associated with anti-PD-1 response. *Nature* **545**, 60–65 (2017).
27. M. Shakiba, P. Zumbo, G. Espinosa-Carrasco, L. Menocal, F. Dündar, S. E. Carson, E. M. Bruno, F. J. Sanchez-Rivera, S. W. Lowe, S. Camara, R. P. Koche, V. P. Reuter, N. D. Socci, B. Whitlock, F. Tamzalit, M. Huse, M. D. Hellmann, D. K. Wells, N. A. Defranoux, D. Betel, M. Philip, A. Schietinger, TCR signal strength defines distinct mechanisms of T cell dysfunction and cancer evasion. *J. Exp. Med.* **219**, e20201966 (2022).
28. H. Li, A. M. van der Leun, I. Yofe, Y. Lubling, D. Gelbard-Solodkin, A. C. J. van Akkooi, M. van den Braber, E. A. Rozeman, J. B. A. G. Haanen, C. U. Blank, H. M. Horlings, E. David, Y. Baran, A. Bercovich, A. Lifshitz, T. N. Schumacher, A. Tanay, I. Amit, Dysfunctional CD8 T cells form a proliferative, dynamically regulated compartment within human melanoma. *Cell* , 775–789.e18 (2019).
29. I. Tirosh, B. Izar, S. M. Prakadan, M. H. Wadsworth II, D. Treacy, J. J. Trombetta, A. Rotem, C. Rodman, C. Lian, G. Murphy, M. Fallahi-Sichani, K. Dutton-Regester, J. R. Lin, O. Cohen, P. Shah, D. Lu, A. S. Genshaft, T. K. Hughes, C. G. K. Ziegler, S. W. Kazer, A. Gaillard, K. E. Kolb, A. C. Villani, C. M. Johannessen, A. Y. Andreev, E. M. van Allen, M. Bertagnolli, P. K. Sorger, R. J. Sullivan, K. T. Flaherty, D. T. Frederick, J. Jané-Valbuena, C. H. Yoon, O. Rozenblatt-Rosen, A. K. Shalek, A. Regev, L. A. Garraway, Dissecting the multicellular ecosystem of metastatic melanoma by single-cell RNA-seq. *Science* **352**, 189–196 (2016).
30. L. E. Lucca, P. P. Axisa, B. Lu, B. Harnett, S. Jessel, L. Zhang, K. Raddassi, L. Zhang, K. Olino, J. Clune, M. Singer, H. M. Kluger, D. A. Hafler, Circulating clonally expanded T cells reflect functions of tumor-infiltrating T cells. *J. Exp. Med.* **218**, e20200921 (2021).
31. B. Bengsch, T. Ohtani, O. Khan, M. Setty, S. Manne, S. O'Brien, P. F. Gherardini, R. S. Herati, A. C. Huang, K. M. Chang, E. W. Newell, N. Bovenschen, D. Pe'er, S. M. Albelda, E. J. Wherry, Epigenomic-guided mass cytometry profiling reveals disease-specific features of exhausted CD8 T cells. *Immunity* **48**, 1029–1045.e5 (2018).
32. E. J. Wherry, S. J. Ha, S. M. Kaech, W. N. Haining, S. Sarkar, V. Kalia, S. Subramaniam, J. N. Blattman, D. L. Barber, R. Ahmed, Molecular signature of CD8+ T cell exhaustion during chronic viral infection. *Immunity* **27**, 670–684 (2007).
33. P. Gueguen, C. Metoikidou, T. Dupic, M. Lawand, C. Goudot, S. Baulande, S. Lameiras, O. Lantz, N. Girard, A. Seguin-Givelet, M. Lefevre, T. Mora, A. M. Walczak, J. J. Waterfall, S. Amigorena, Contribution of resident and circulating precursors to tumor-infiltrating CD8(+) T cell populations in lung cancer. *Sci. Immunol.* **6**, eabd5778 (2021).
34. D. Bending, A. Paduraru, C. B. Ducker, P. Prieto Martín, T. Crompton, M. Ono, A temporally dynamicFoxp3autoregulatory transcriptional circuit controls the effector T_{reg} programme. *EMBO J.* **37**, e99013 (2018).
35. T. Torcellan, H. R. Hampton, J. Bailey, M. Tomura, R. Brink, T. Chtanova, In vivo photolabeling of tumor-infiltrating cells reveals highly regulated egress of T-cell subsets from tumors. *Proc. Natl. Acad. Sci. U.S.A.* **114**, 5677–5682 (2017).
36. C. Gerlach, E. A. Moseman, S. M. Loughhead, D. Alvarez, A. J. Zwijnenburg, L. Waanders, R. Garg, J. C. de la Torre, U. von Andrian, The chemokine receptor CX3CR1 defines three antigen-experienced CD8 T cell subsets with distinct roles in immune surveillance and homeostasis. *Immunity* **45**, 1270–1284 (2016).
37. Y. Farsakoglu, B. McDonald, S. M. Kaech, Motility matters: How CD8(+) T-cell trafficking influences effector and memory cell differentiation. *Cold Spring Harb. Perspect. Biol.* **13**, a038075 (2021).
38. S. J. Im, M. Hashimoto, M. Y. Gerner, J. Lee, H. T. Kissick, M. C. Burger, Q. Shan, J. S. Hale, J. Lee, T. H. Nasti, A. H. Sharpe, G. J. Freeman, R. N. Germain, H. I. Nakaya, H. H. Xue, R. Ahmed, Defining CD8+ T cells that provide the proliferative burst after PD-1 therapy. *Nature* **537**, 417–421 (2016).

39. L. Kok, F. E. Dijkgraaf, J. Urbanus, K. Bresser, D. W. Vredevoogd, R. F. Cardoso, L. Perié, J. B. Beltman, T. N. Schumacher, A committed tissue-resident memory T cell precursor within the circulating CD8+ effector T cell pool. *J. Exp. Med.* **217**, e20191711 (2020).
40. L. Zhang, X. Yu, L. Zheng, Y. Zhang, Y. Li, Q. Fang, R. Gao, B. Kang, Q. Zhang, J. Y. Huang, H. Konno, X. Guo, Y. Ye, S. Gao, S. Wang, X. Hu, X. Ren, Z. Shen, W. Ouyang, Z. Zhang, Lineage tracking reveals dynamic relationships of T cells in colorectal cancer. *Nature* **564**, 268–272 (2018).
41. T. D. Wu, S. Madireddi, P. E. de Almeida, R. Banchereau, Y. J. J. Chen, A. S. Chitre, E. Y. Chiang, H. Iftikhar, W. E. O'Gorman, A. Au-Yeung, C. Takahashi, L. D. Goldstein, C. Poon, S. Keerthivasan, D. E. de Almeida Nagata, X. du, H. M. Lee, K. L. Banta, S. Mariathasan, M. das Thakur, M. A. Huseni, M. Ballinger, I. Estay, P. Caplazi, Z. Modrusan, L. Delamarre, I. Mellman, R. Bourgon, J. L. Grogan, Peripheral T cell expansion predicts tumour infiltration and clinical response. *Nature* **579**, 274–278 (2020).
42. H. Huang, C. Wang, F. Rubelt, T. J. Scriba, M. M. Davis, Analyzing the Mycobacterium tuberculosis immune response by T-cell receptor clustering with GLIPH2 and genome-wide antigen screening. *Nat. Biotechnol.* **38**, 1194–1202 (2020).
43. D. T. Fearon, Seeking wisdom in innate immunity. *Nature* **388**, 323–324 (1997).
44. E. W. Roberts, A. Deonarine, J. O. Jones, A. E. Denton, C. Feig, S. K. Lyons, M. Espeli, M. Kraman, B. McKenna, R. J. B. Wells, Q. Zhao, O. L. Caballero, R. Larder, A. P. Coll, S. O'Rahilly, K. M. Brindle, S. A. Teichmann, D. A. Tuveson, D. T. Fearon, Depletion of stromal cells expressing fibroblast activation protein-α from skeletal muscle and bone marrow results in cachexia and anemia. *J. Exp. Med.* **210**, 1137–1151 (2013).
45. M. Bellone, D. Cantarella, P. Castiglioni, M. C. Crosti, A. Ronchetti, M. Moro, M. P. Garancini, G. Casorati, P. Dellabona, Relevance of the tumor antigen in the validation of three vaccination strategies for melanoma. *J. Immunol.* **165**, 2651–2656 (2000).
46. D. A. Bolotin, S. Poslavsky, I. Mitrophanov, M. Shugay, I. Z. Mamedov, E. V. Putintseva, D. M. Chudakov, MiXCR: Software for comprehensive adaptive immunity profiling. *Nat. Methods* **12**, 380–381 (2015).
47. K. E. Yost, A. T. Satpathy, D. K. Wells, Y. Qi, C. Wang, R. Kageyama, K. L. McNamara, J. M. Granja, K. Y. Sarin, R. A. Brown, R. K. Gupta, C. Curtis, S. L. Bucktrout, M. M. Davis, A. L. S. Chang, H. Y. Chang, Clonal replacement of tumor-specific T cells following PD-1 blockade. *Nat. Med.* **25**, 1251–1259 (2019).
48. J. C. Beltra, S. Manne, M. S. Abdel-Hakeem, M. Kurachi, J. R. Giles, Z. Chen, V. Casella, S. F. Ngiow, O. Khan, Y. J. Huang, P. Yan, K. Nzingha, W. Xu, R. K. Amaravadi, X. Xu, G. C. Karakousis, T. C. Mitchell, L. M. Schuchter, A. C. Huang, E. J. Wherry, Developmental relationships of four exhausted CD8(+) T cell subsets reveals underlying transcriptional and epigenetic landscape control mechanisms. *Immunity* **52**, 825–841.e8 (2020).
49. M. Ziemann, MSigDB gene sets for mouse (2016); https://genomespot.blogspot.com/2016/12/msigdb-gene-sets-for-mouse.html.
50. N. Borcherding, N. L. Bormann, G., scRepertoire: An R-based toolkit for single-cell immune receptor analysis. *F1000Res* **9**, 47 (2020).
51. T. Stuart, A. Butler, P. Hoffman, C. Hafemeister, E. Papalexi, W. M. Mauck III, Y. Hao, M. Stoeckius, P. Smibert, R. Satija, Comprehensive integration of single-cell data. *Cell* **177**, 1888–1902.e21 (2019).
52. F. A. Wolf, P. Angerer, F. J. Theis, SCANPY: Large-scale single-cell gene expression data analysis. *Genome Biol.* **19**, 15 (2018).
53. A. Butler, P. Hoffman, P. Smibert, E. Papalexi, R. Satija, Integrating single-cell transcriptomic data across different conditions, technologies, and species. *Nat. Biotechnol.* **36**, 411–420 (2018).
54. J. H. Levine, E. F. Simonds, S. C. Bendall, K. L. Davis, E. A. D. Amir, M. D. Tadmor, O. Litvin, H. G. Fienberg, A. Jager, E. R. Zunder, R. Finck, A. L. Gedman, I. Radtke, J. R. Downing, D. Pe'er, G. P. Nolan, Data-driven phenotypic dissection of AML reveals progenitor-like cells that correlate with prognosis. *Cell* **162**, 184–197 (2015).
55. V. D. Blondel, J.-L. Guillaume, R. Lambiotte, E. Lefebvre, Fast unfolding of communities in large networks. *J. Stat. Mech Theory Exper.* **2008**, P10008 (2008).
56. J. Cao, M. Spielmann, X. Qiu, X. Huang, D. M. Ibrahim, A. J. Hill, F. Zhang, S. Mundlos, L. Christiansen, F. J. Steemers, C. Trapnell, J. Shendure, The single-cell transcriptional landscape of mammalian organogenesis. *Nature* **566**, 496–502 (2019).
57. M. Takahashi, Intratumoral antigen-signaling traps CD8+ T Cells to confine exhaustion to the tumor site, 1.0.0, *Zenodo*; doi:10.5281/zenodo.11057548.
58. J. A. Pai, A. T. Satpathy, High-throughput and single-cell T cell receptor sequencing technologies. *Nat. Methods* **18**, 881–892 (2021).
59. A. H. Wagner, B. Walsh, G. Mayfield, D. Tamborero, D. Sonkin, K. Krysiak, J. Deu-Pons, R. P. Duren, J. Gao, J. M. Murry, S. Patterson, C. del Vecchio Fitz, B. A. Pitel, O. U. Sezerman, K. Ellrott, J. L. Warner, D. T. Rieke, T. Aittokallio, E. Cerami, D. I. Ritter, L. M. Schriml, R. R. Freimuth, M. Haendel, G. Raca, S. Madhavan, M. Baudis, J. S. Beckmann, R. Dienstmann, D. Chakravarty, X. S. Li, S. Mockus, O. Elemento, N. Schultz, N. Lopez-Bigas, M. Lawler, J. Goecks, M. Griffith, O. L. Griffith, A. A. Margolin, Variant Interpretation for Cancer Consortium, A harmonized meta-knowledgebase of clinical interpretations of somatic genomic variants in cancer. *Nat. Genet.* **52**, 448–457 (2020).
60. E. Becht, L. M. Innes, J. Healy, C.-A. Dutertre, I. W. H. Kwok, L. G. Ng, F. Ginhoux, E. W. Newell, Dimensionality reduction for visualizing single-cell data using UMAP. *Nat. Biotechnol.* **37**, 38–44 (2019).
61. D. van Dijk, R. Sharma, J. Nainys, K. Yim, P. Kathail, A. J. Carr, C. Burdziak, K. R. Moon, C. L. Chaffer, D. Pattabiraman, B. Bierie, L. Mazutis, G. Wolf, S. Krishnaswamy, D. Pe'er, Recovering gene interactions from single-cell data using data diffusion. *Cell* **174**, 716–729.e27 (2018).
62. M. D. Luecken, F. J. Theis, Current best practices in single-cell RNA-seq analysis: A tutorial. *Mol. Syst. Biol.* **15**, e8746 (2019).
63. W. S. Cleveland, Robust locally weighted regression and smoothing scatterplots. *J. Am. Stat. Assoc.* **74**, 829–836 (1979).
64. H. Kibirige, scikit-misc, version 0.5.2, *GitHub Repository* (2023); https://github.com/has2k1/scikit-misc.
65. M. Löning, A. Bagnall, S. Ganesh, V. Kazakov, J. Lines, F. J. Király, sktime: A unified interface for machine learning with time series. arXiv:1909.07872 (2019). https://arxiv.org/abs/1909.07872.
66. L. Zappia, B. Phipson, A. Oshlack, Splatter: Simulation of single-cell RNA sequencing data. *Genome Biol.* **18**, 174 (2017).

Acknowledgments: We thank M. Barile and X, Wang from the Gottgens group for insights into single-cell analysis. We thank A. Lund for sharing experimental protocols. We thank the Core Facilities at the Cancer Research UK Cambridge Institute (Li Ka Shing Centre), including the Biological Resources Unit, Research Instrumentation & Cell Services, Light Microscopy, and Flow Cytometry, for technical provision. **Funding:** This work has been funded by the Medical Research Council (MC_UU_0025/12) and Medical Research Foundation (MRF-057-0002-RG-THAV-C0798) awards to J.E.D.T. From April 2019, the core grant to the CI was C9545/A29580. The Li Ka Shing Centre where components of this work were performed was funded by CK Hutchison Holdings Limited, the University of Cambridge, Cancer Research UK, the Atlantic Philanthropies, and others. M.T. was supported by the Masason Foundation, the Recruit Foundation, and the Gates Cambridge Trust. T.Y.F.H. is funded by the Royal Society, Wellcome Trust (204622/Z/16/Z), and Cancer Research UK (CRUK) core award (A24995). **Author contributions:** J.E.D.T. designed the AgRSR mouse. M.T. and T.Y.S. conducted the experiments with the assistance of V.C.-E., R.H., J.C.Y-P., K.K., M.R., and T.M. M.T. conducted the computational analysis with the assistance of V.C.-E. All authors contributed to the analysis of the presented results. M.T. and J.E.D.T. wrote the paper with input from all other authors. J.E.D.T. supervised the work with the assistance of P.A.L. and M.A.C. **Competing interests:** J.E.D.T. is a cofounder of CamBiotics. K.O. is on the scientific advisory boards of Macomics and Ionctura and provides paid consultancy to those companies. K.O. receives research funding from AstraZeneca. R.R. holds or has held paid consultancies with Lyell Immunopharma, Achilles Therapeutics, and Enhanc3D Genomics. R.R. is a principal investigator of research projects funded by AstraZeneca and F-star Therapeutics on unrelated topics that do not constitute competing interests. R.R. is an inventor on patent/patent application 2401216.3 held/submitted by University of Cambridge that covers the use of transcription factors to enhance the persistence and long-term efficacy of CAR T cell therapy. The other authors declare that they have no competing interests. **Data and materials availability:** Sequence data that support the findings of this study have been deposited in the Gene Expression Omnibus database (GEO: GSE266360 and GSE266361). Code for next-generation sequencing analysis and TrajClust is deposited on Zenodo (https://doi.org/10.5281/zenodo.11057548) (*57*) and GitHub (https://github.com/MunetomoT/TrajClust), respectively. Raw data are included in data file S2. Additional information and materials will be made available upon request.

Submitted 1 August 2022
Resubmitted 10 November 2023
Accepted 2 May 2024
Published 24 May 2024
10.1126/sciimmunol.ade2094